

Cooperative “folding transition” in the sequence space facilitates function-driven evolution of protein families

Akira R. Kinjo

Institute for Protein Research, Osaka University, 3-2 Yamadaoka, Suita, Osaka, 565-0871, Japan

Abstract

In the protein sequence space, natural proteins form clusters of families which are characterized by their unique native folds whereas the great majority of random polypeptides are neither clustered nor foldable to unique structures. Since a given polypeptide can be either foldable or unfoldable, a kind of “folding transition” is expected at the boundary of a protein family in the sequence space. By Monte Carlo simulations of a statistical mechanical model of protein sequence alignment that coherently incorporates both short-range and long-range interactions in addition to variable-length insertions, we demonstrate the existence of such transition between natural-like sequences and random sequences in the sequence subspaces for 15 domain families. The transition was found to be highly cooperative and two-state-like. Furthermore, enforcing or suppressing consensus residues on a few of the well-conserved sites enhanced or diminished, respectively, the natural-like pattern formation over the entire sequence. In most families, the key sites included ligand binding sites. These results suggest some selective pressure on the key residues, such as ligand binding activity, may cooperatively facilitate the emergence of a protein family during evolution. From a more practical aspect, the present results highlight an essential role of long-range effects in precisely defining protein families, which are absent in conventional sequence models.

Keywords: protein folding, molecular evolution, protein design, sequence analysis, Monte Carlo simulation

1. Introduction

Natural proteins can be classified into families based on their sequence similarity (Finn et al., 2014). This is considered to be primarily a consequence of molecular evolution: proteins evolved from a common ancestral protein share similar sequences. However, evolution alone does not account for the existence of relatively well-defined (domain) families that are distributed rather discretely than continuously in the sequence space (Maynard Smith, 1970; Nishikawa, 1993, 2002; Goldstein, 2008). A key to understanding the family distribution is protein folding. As observed in protein structure classification databases (Murzin et al., 1995; Orengo et al., 1997; Cheng et al., 2014), each protein family corresponds to a unique three-dimensional fold, suggesting the existence of physical constraints imposed on protein sequences during the evolutionary process to maintain the fold (Morcos et al., 2014). While protein structures can tolerate great many mutations to the extent that proteins with little sequence similarity can share the same fold, residue conservation patterns reflect the structural context of protein sequences. This fact has long been exploited in protein structure prediction in the form of position-specific scoring matrices

(Taylor, 1986; Gribskov et al., 1987; Kinjo and Nakamura, 2008) and, more recently, direct-coupling analysis and related methods (Balakrishnan et al., 2011; Morcos et al., 2011; Jones et al., 2012; Taylor et al., 2012; Miyazawa, 2013; Kinjo, 2015; Levy et al., 2017).

Under a given physiological condition, a polypeptide is either able or unable to fold into some unique structure. This suggests the existence of a “folding transition” at the border between an “island” of a protein family and the “sea” of random polypeptide, that is analogous to the folding transition of a protein molecule in the conformational space (Nishikawa, 1993, 2002). It should be noted, however, that there are many families in the sequence space so that a sequence moving in the sequence space may fall into any one of these families. This is in contrast to protein folding in the conformational space where there is usually only one unique native structure for a given protein sequence. Therefore, the system in which the analogy of protein folding holds should be limited to the vicinity of each protein family rather than the entire sequence space. In the following, we focus on the folding transition in a sequence subspace around a given protein family.

There have been a number of theoretical and computational studies on subjects related to the sequence space such as foldability (Shakhnovich and Gutin, 1993; Govindarajan and Goldstein, 1995; Morcos et al., 2014), molecular evolution within an island (Bornberg-Bauer and Chan,

Email address: akinjo@protein.osaka-u.ac.jp (Akira R. Kinjo)

1999; Bastolla et al., 1999; Wroe et al., 2005) and between islands (Wroe et al., 2007; Holzgräfe and Wallin, 2014; Sikosek et al., 2016), or the size and/or distribution of islands in the sequence space (Govindarajan and Goldstein, 1996; Li et al., 1996; Bornberg-Bauer, 1997; Kuhlman and Baker, 2000; Koehl and Levitt, 2002). On the contrary, little attention has been paid to the transition between an island (a set of sequences belonging to the same family) and the sea (the set of sequences that don't belong to the family). Nevertheless, characterizing the folding transition in the sequence space may help understand essential features that constitute a protein family and possible evolutionary trajectories that may have led to the emergence of a protein family. It also has practical importance in identifying new family members and designing new proteins.

In the following, we investigate the folding transition in the sequence subspaces for 15 protein domain families by performing extensive Monte Carlo (MC) simulations of the modified lattice gas model (LGM) of protein sequence alignment (Kinjo, 2016, 2017) that coherently integrates long-range interactions and variable-length insertions. Using the LGM, the existence of a sharp two-state transition in the sequence subspace is demonstrated. Furthermore, the nature of the transition is examined in detail by analyzing residue distribution of each site along the transition as well as by performing virtual “mutation” experiments.

2. Theory

We briefly summarize the theory to the extent that is necessary for understanding the present study. For more details about the formulation of the LGM as well as the algorithms for MC simulations and parameter optimization, refer to the previous papers (Kinjo, 2016, 2017). The LGM for a given Pfam (Finn et al., 2014) family consists of N “core” sites and $N - 1$ “insert” sites which respectively correspond to the “match” states and “insert” states of the Pfam profile hidden Markov model (HMM) of length N , excluding the N- and C-terminal insert states. Exactly one of the 21 residue types (including the “delete” symbol) can exist on each core site whereas arbitrarily many (including zero) residues out of the standard 20 residue types can reside at each insert site. The array of core and insert sites are connected via “bonds” (solid arrows in Fig. 1) that reflect the linear polypeptide structure. A pair of model sites connected via a bond are called a “bonded pair” in the following. Between core sites more than 2 residues apart along the sequence, there may be interactions (dashed lines in Fig. 1) based on a representative native structure of the family. Two sites are defined to be interacting if the residues aligned to those sites are in contact in the corresponding representative native structure. Two residues are defined to be in contact if any non-hydrogen atoms in those residues are within 5\AA . Interactions are defined only

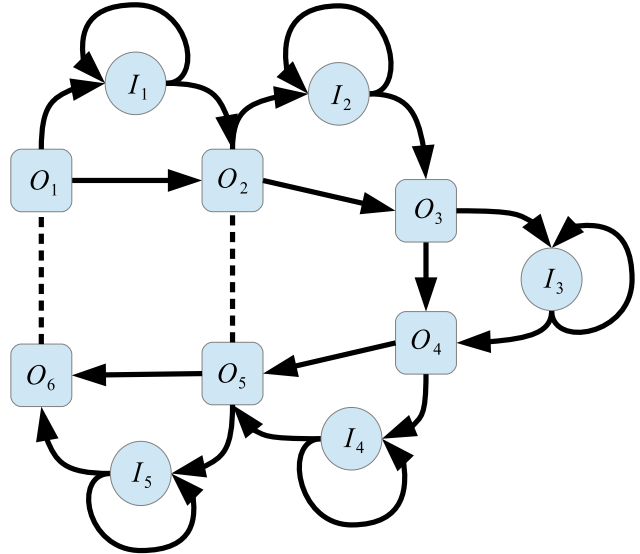


Figure 1: An example model structure with model length $N = 6$. There are N core sites O_1, \dots, O_N and $N - 1$ insert sites I_1, \dots, I_{N-1} . These model sites are bonded via “bonds” (solid arrows). Some pairs of non-bonded core sites may be “interacting” (dashed lines).

between core sites for simplicity. Interacting core sites are referred to as “non-bonded” pairs in the following.

Let $\mathbf{a} = a_1 \dots a_L$ be an amino acid sequence of L residues and an LGM \mathcal{M} of length N consist of core sites O_1, \dots, O_N and insert sites I_1, \dots, I_{N-1} . An alignment between the sequence \mathbf{a} and the model \mathcal{M} is represented as a sequence of pairs of a model site (core or insert) and a residue: $\mathbf{X} = X_1 \dots X_{L_{\mathbf{X}}}$ where $L_{\mathbf{X}}$ is the length of the alignment and each X_i is a pair such as (S, a) with $S \in \{O_i\}_{i=1, \dots, N} \cup \{I_i\}_{i=1, \dots, N-1}$ and $a \in \{a_1, \dots, a_L\}$. For example, given an amino acid sequence, say KCFPDGVW, and a model of length $N = 6$ (Fig. 1), one of many possible alignments is represented as $\mathbf{X} = X_1 \dots X_9 = (O_1, \text{K}) (O_2, \text{C}) (O_3, \text{F}) (I_3, \text{P}) (I_3, \text{D}) (I_3, \text{G}) (O_4, -) (O_5, \text{V}) (O_6, \text{W})$. Note there are multiple occurrence of the insert site I_3 whereas other insert sites are completely absent in this particular alignment. Since there may be any number of residues at each insert site, the alignment length is variable.

Based on this representation of sequence alignment, the energy function of alignment \mathbf{X} is defined as

$$E(\mathbf{X}) = - \sum_{k=1}^{L_{\mathbf{X}}-1} J(X_k, X_{k+1}) - \sum_{(k,l) \in \mathcal{T}} K(X_k, X_l) - \sum_{k=1}^{L_{\mathbf{X}}} \mu(X_k) \quad (1)$$

where J and K are short-range and long-range interaction parameters, respectively, μ 's are chemical potentials, and \mathcal{T} indicates the set of all the interacting non-bonded pairs. The short-range interactions act only between bonded pairs of residues that are consecutive in the alignment (i.e.,

between X_k and X_{k+1} in Eq. 1). The long-range interactions act between residues that are aligned to interacting non-bonded pairs. The chemical potentials are so called because they are used to control the residue densities of each site. Only J and K parameters constitute intrinsic energy, and they are to be determined from a given (observed) multiple sequence alignment (MSA) of the family sequences (see below).

We assume that the probability $P(\mathbf{X})$ of obtaining an alignment \mathbf{X} is given by the Boltzmann distribution:

$$P(\mathbf{X}) = \frac{\exp[-E(\mathbf{X})/T]}{\Xi[T]} \quad (2)$$

where T is the “(design) temperature” (Pande et al., 2000) in energy unit and $\Xi[T]$ is the partition function

$$\Xi[T] = \sum_{\mathbf{X}} \exp[-E(\mathbf{X})/T]. \quad (3)$$

Here, the summation is over all possible alignments (\mathbf{X}) of all possible amino acid sequences with the model. Since the alignment length can vary, this ensemble is considered to be a grand canonical ensemble.

Given the parameters J , K and μ , we can sample (alignments of) sequences according to the probability distribution Eq. (2) by running grand canonical Monte Carlo (MC) simulations (Kinjo, 2017).

We define the *standard condition* as the system with $\mu(X_k) = 0$ for all X_k (i.e., no perturbation), and the *natural condition* as the standard condition with $T = 1$. The parameters J and K are determined iteratively so that the pair number densities of residues for bonded and non-bonded pairs over the samples produced by MC simulations under the natural condition match those observed in the given MSA (Lapedes et al., 1999; Sutto et al., 2015). This optimization corresponds to minimizing the following free energy function under the natural condition ($T = 1$ in particular):

$$F[T] = -\max_{J,K} (\langle E \rangle_{\text{obs}} - \Omega[T]) \quad (4)$$

where $\langle E \rangle_{\text{obs}}$ is the average energy of the observed MSA and $\Omega[T] = -T \ln \Xi[T]$ is the grand potential. It can be easily shown that this is equivalent to the principle of maximum entropy (Morcos et al., 2011).

The design temperature in the LGM controls the mutation rate uniformly over the entire sites. The higher the temperature, the higher the mutation rate. The mutation rate here means the number of accepted mutations per attempted mutation, and mutations are attempted at a constant time interval. The relationship between the present “energy” and physical folding free energy has been recently established by Miyazawa (2017).

3. Results

3.1. Sequence pattern formation is accompanied by a cooperative two-state transition

We have determined the energy parameters for each of the 15 families of relatively small domains listed in Table 1 by using MC simulations following the procedure described previously (Kinjo, 2017).

Using the optimized parameters, we run a multicanonical MC simulation (Berg and Neuhaus, 1992) for each family from which the specific heat,

$$C(T) = \frac{\langle E^2 \rangle_T - \langle E \rangle_T^2}{T^2}, \quad (5)$$

was computed as a function of temperature (Fig. 2A). For all the families but HATPase_c, a single peak in the specific heat was observed, indicating the existence of a transition. An increase in the specific heat of HATPase_c at higher temperatures was due to excessively long insertions. Depending on the family, the peak temperature (T_m ; see Table 1) ranged between $T = 1.009$ (for DnaB) and $T = 1.033$ (for zf-C2H2). The energy distribution obtained from grand canonical MC simulations at T_m (Fig. 2B) showed a clear two-state transition between low energy and high energy states.

In order to confirm if the low-energy sequences are indeed similar to the natural sequences, we compared the profile HMM of each family against the set of sequences generated by the MC simulations. Out of 10,000 sequences generated at each temperature ranging from $T = 0.95$ to $T = 1.05$, a profile HMM search was performed (using the `hmmsearch` program (Eddy, 2011)) to identify the sequences that significantly matched the Pfam profile HMM with full sequence E-value < 0.01 (Fig. 2C). The hit ratio (the fraction of sequences significantly similar to the family’s profile HMM) shows the clear two-state transition between natural-like sequences and non-natural-like (\approx random) sequences around the transition temperature T_m for each family, and the sequences generated at lower temperatures were indeed more similar to natural sequences. Since these natural-like sequences are expected to fold into the native fold of the domain family but non-natural-like sequences are not, this transition can be regarded as a “folding transition” in the sequence subspace. The hit rates at $T = 1$ (the natural condition) ranged from 73.3% (for zf-C2H2) and 92.5% (for HATPase_c), indicating there were a non-negligible fraction of non-natural-like sequences at the natural condition. In particular, the C2H2-type zinc finger domain (zf-C2H2) consisting of only 23 core sites exhibited a large fraction of non-natural-like sequences at lower temperature. For all the families examined, the hit ratio was a decreasing function of temperature. For later reference, we defined a “disordering temperature”, T_D , of each family as the lowest temperature at which the hit ratio was less than 1% (column “ T_D ” in Table 1).

Table 1: Pfam domain families used in the study.

Pfam ID	description	N^a	MSA ^b	M^c	PDB ^d	T_D^e	T_m^f
zf-C2H2	Zinc finger, C2H2 type	23	uniprot	503700	4m9vC	1.085	1.033
SH3_1	SH3 domain	48	uniprot	30001	4hvuA	1.050	1.019
HTH_3	Helix-turn-helix	55	uniprot	97452	1r69A	1.045	1.019
Homeobox	Homeobox domain	57	uniprot	47752	4rduD	1.040	1.015
HisKA	His Kinase A (phospho-acceptor) domain	64	uniprot	224625	2c2aA	1.045	1.018
RRM_1	RNA recognition motif. (a.k.a. RRM, RBD, or RNP domain)	70	uniprot	124098	1l3kA	1.045	1.018
PDZ	PDZ domain (Also known as DHR or GLGF)	82	uniprot	34441	1g9oA	1.035	1.013
fn3	Fibronectin type III domain	85	uniprot	104374	2ic2A	1.050	1.019
I-set	Immunoglobulin I-set domain	90	uniprot	93895	1u2hA	1.035	1.014
OmpA	OmpA family	95	uniprot	44148	4zhwA	1.025	1.010
DnaB	DnaB-like helicase N terminal domain	103	uniprot	14624	2r5uA	1.030	1.009
V-set	Immunoglobulin V-set domain	109	uniprot	10392	4unuA	1.035	1.012
Globin	Globin	110	uniprot	6055	2nrlA	1.030	1.011
HATPase_c	Histidine kinase-, DNA gyrase B-, and HSP90-like ATPase	111	rp55	106253	4xe2A	1.030	1.011
Response_reg	Response regulator receiver domain	112	full	98600	3chyA	1.025	1.010

^aLength of Pfam profile HMM. ^bDataset for Pfam multiple sequence alignment. ^cNumber of sequences in the MSA with less than 10% deletes. ^dPDB (Berman et al., 2007) chains used for computing three-dimensional contacts. References: 4m9v (Liu et al., 2013); 4hvu (Bacarizo and Camara-Artigas, 2013); 1r69 (Mondragon et al., 1989); 4rdu (JCSG and STEMCELL, 2014); 2c2a (Marina et al., 2005); 1l3k (Vitali et al., 2002); 1g9o (Karthikeyan et al., 2001); 2ic2 (McLellan et al., 2006); 1u2h (Manjasetty et al., 2005); 4zhw (Li et al., 2015); 2r5u (Biswas and Tsodikov, 2008); 4unu (Brumshtein et al., 2014); 2nrl (Schreiter et al., 2007); 4xe2 (Raman et al., 2015); 3chy (Volz and Matsumura, 1991). ^eDisordering temperature. ^fTransition temperature.

3.2. Less conserved sites order at higher temperatures, better conserved sites order at lower temperatures

Next, the transition was characterized in terms of residue distribution at each site over a temperature range. The “naturalness” of each core site of simulated sequences at a given temperature was evaluated by the Kullback-Leibler divergence (MacKay, 2003) $D_{O_i}(T)$:

$$D_{O_i}(T) = \sum_{a=1}^{21} \langle n_{(O_i,a)} \rangle_T \log \frac{\langle n_{(O_i,a)} \rangle_T}{\langle n_{(O_i,a)} \rangle_{\text{obs}}} \quad (6)$$

which measures the difference between the residue distribution $\langle n_{(O_i,a)} \rangle_T$ of the site O_i at temperature T from the observed residue distribution $\langle n_{(O_i,a)} \rangle_{\text{obs}}$. An example for the SH3 domain is provided in Fig. 3C. Lower divergence values imply more natural-likeness. By construction, the divergence is nearly 0 for all the sites at $T = 1$, but the values varied largely among different sites for higher temperatures. In general, better conserved sites (c.f., Fig. 3A) have larger divergence at high temperatures. In the following, we use the $D_{O_i}(T_D)$, i.e., divergence at the disordering temperature $T = T_D$, as a measure of conservation. As expected, sites with a larger contact number (Kinjo et al., 2005) (i.e., the number of non-bonded contacts a site makes with other sites; see Fig. 3B for example) tend to be more conserved as can be seen in their correlations (Fig. 4A).

Ordering of each site can be quantified via the derivative of the divergence with respect to temperature (c.f., Fig. 3D):

$$\begin{aligned} C_{O_i}(T) &= \frac{dD_{O_i}(T)}{dT} \\ &= \frac{1}{T^2} \sum_{a=1}^{21} [\langle n_{(O_i,a)} E \rangle_T - \langle n_{(O_i,a)} \rangle_T \langle E \rangle_T] \\ &\quad \times \log \left[\frac{\langle n_{(O_i,a)} \rangle_T}{\langle n_{(O_i,a)} \rangle_{\text{obs}}} \right] \end{aligned} \quad (7)$$

which we call “differential divergence” in the following. Note that this is a weighted sum of covariance between the number density and total energy where the unnormalized and signed weights are $\log[\langle n_{(O_i,a)} \rangle_T / \langle n_{(O_i,a)} \rangle_{\text{obs}}]$. Thus, the peaks of this quantity provide the site-specific transition point at which a large change in the residue distribution is accompanied with a large change in total energy. Precisely, the site-wise transition temperature T_{m,O_i} is defined by

$$T_{m,O_i} = \arg \max_{T < T_D} C_{O_i}(T) \quad (8)$$

(see Fig. 3E for an example). For some sites, this temperature cannot be defined because of the absence of a unique peak for $T < T_D$ (due to lack of non-bonded interactions; this was observed for several sites of the fn3 family). The range of the site-wise transition temperatures are plotted along with T_m and T_D in Fig. 4B. The site-wise temperatures all appeared slightly above the global

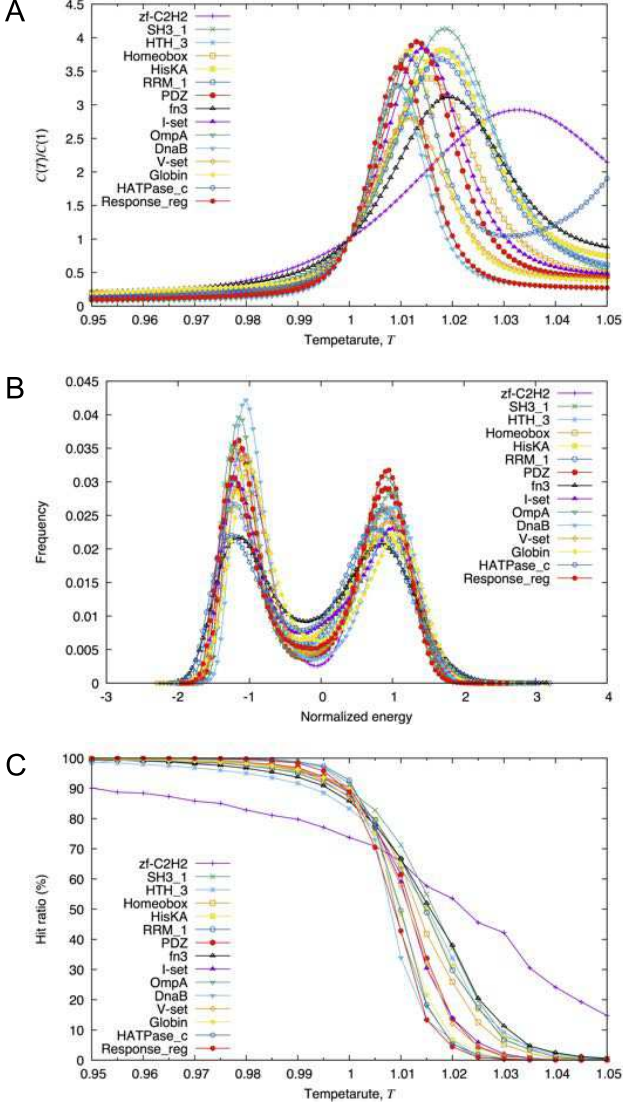


Figure 2: Results of simulations. (A) The specific heat obtained from multicanonical simulations [normalized by $C(T = 1)$]. (B) The energy distributions of grand canonical ensembles at transition temperatures (the energy is normalized by its average and standard deviation at $T = T_m$ for each family). (C) The “hit ratio”, the fraction of the sequences generated by MC simulations at various temperatures that significantly match to the profile HMMs.

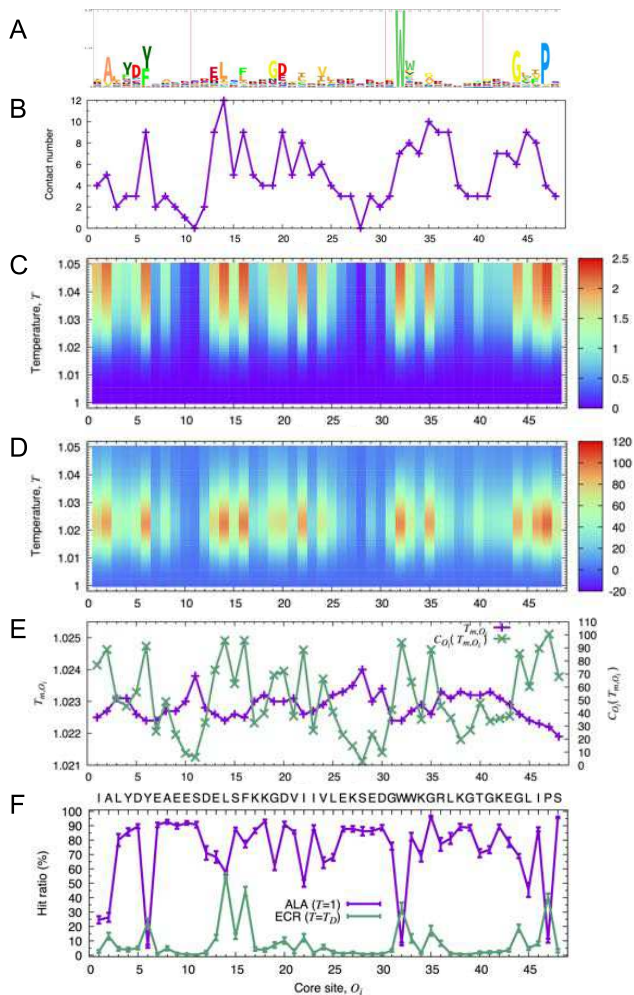


Figure 3: Site-wise properties for the Pfam SH3_1 family. In all the panels, the horizontal axis represents core sites. (A) The HMM logo taken from the Pfam site (<http://pfam.xfam.org/family/PF00018#tabview=tab4>). (B) The contact number of core sites (i.e., the number of non-bonded interactions each site makes with other sites based on the reference structure). (C) The divergence map, $D_{O_i}(T)$. (D) The differential divergence map $C_{O_i}(T) = dD_{O_i}(T)/dT$. (E) Site-wise transition temperature T_{m,O_i} (left ordinate) and the differential divergence at the temperature $C_{O_i}(T_{m,O_i})$ (right ordinate). (F) Virtual “mutation” experiments: “alanine” scanning (ALA) and “enforcedly conserved residue” scanning (ECR) (see text for the details).

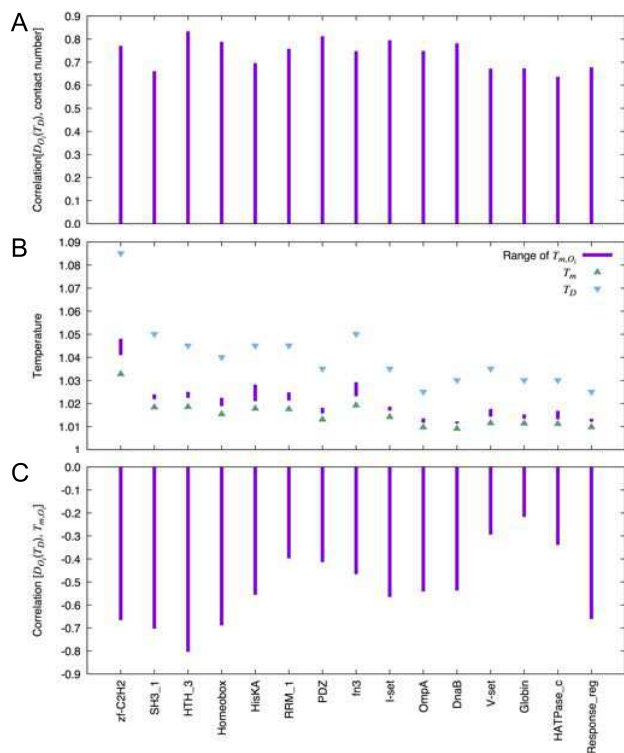


Figure 4: Site-wise properties. (A) Correlation between site conservation $D_{O_i}(T_D)$ and contact number. (B) Range of site-wise transition temperatures T_{m,O_i} together with the global transition temperature T_m and disordering temperature T_D . (C) Correlation between the site-wise temperatures T_{m,O_i} and site conservation $D_{O_i}(T_D)$.

transition temperature T_m , indicating a global (higher order) ordering process between the minimum T_{m,O_i} and T_m . The site-wise transition temperature was found to be negatively correlated with site conservation $D_{O_i}(T_D)$ (Fig. 4C) although the correlation was not always significant. Thus, as temperature lowers, local ordering starts from less conserved sites, but these sites have little global effects (smaller values of $C_{O_i}(T_{m,O_i})$; see Fig. 3E, green line), then it proceeds to increasingly better conserved sites with increasingly greater effects (larger change in total energy). Then, higher-order ordering proceeds down to the global transition temperature, T_m . Interestingly, a nearly perfect correlation ($R \approx 1$) was found between $\{C_{O_i}(T_m)\}$ and $\{D_{O_i}(T_D)\}$. Thus, the transition of each site appears almost completely determined by the conservation patterns.

3.3. Suppressing key residues inhibits sequence pattern formation under the natural condition: “Alanine” scanning

Although the above analysis of divergence maps hinted some differential roles of individual sites in determining natural-like sequences, the site-wise transition temperature T_{m,O_i} did not vary much across the sites. In order to explore the role of each site more directly, we performed virtual site-directed mutation experiments by manipulating the chemical potential μ . First, we performed “alanine” scanning experiments. That is, for each core site O_i , the chemical potential for alanine (“A”) residue (or glycine “G” if the consensus residue was alanine) was set to a large positive value (namely, $\mu(O_i, A) = +20$) while other μ 's were set to 0. This effectively fixes alanine residue at the site O_i while allowing other sites to freely adopt residues that are consistent with the perturbation. By performing MC simulations at $T = 1$ and applying the hmmsearch program to the sampled sequences, the hit ratio $h_{O_i}^{ALA}$ (the fraction of natural-like sequences) of the “alanine mutant” was determined (c.f., Fig. 3C, magenta line). This hit ratio was compared to the hit ratio $h_0(T = 1)$ of the natural condition (c.f., Fig. 2C). Namely, we evaluated the “mutants” in terms of the following enrichment value:

$$\text{En}_{O_i}^{ALA} = h_{O_i}^{ALA} / h_0(T = 1). \quad (9)$$

While most of the sites were not largely affected by alanine mutations (the enrichment ranging between 0.5 and 1.5), a few sites exhibited enrichment of less than 0.5 (Fig. 5A), that is, the fraction of natural-like sequences for these few mutants was less than a half of that under the natural condition. The hit ratio of mutants $\{h_{O_i}^{ALA}\}_{i=1,\dots,N}$ and a measure of conservation of each site $\{D_{O_i}(T_D)\}_{i=1,\dots,N}$ showed negative correlations (Fig. 5C; $R < -0.50$ for most families), indicating better conserved sites are affected more severely by the alanine mutation. This result suggests that fixation of some key residues is essential for the global pattern formation of natural-like sequences.

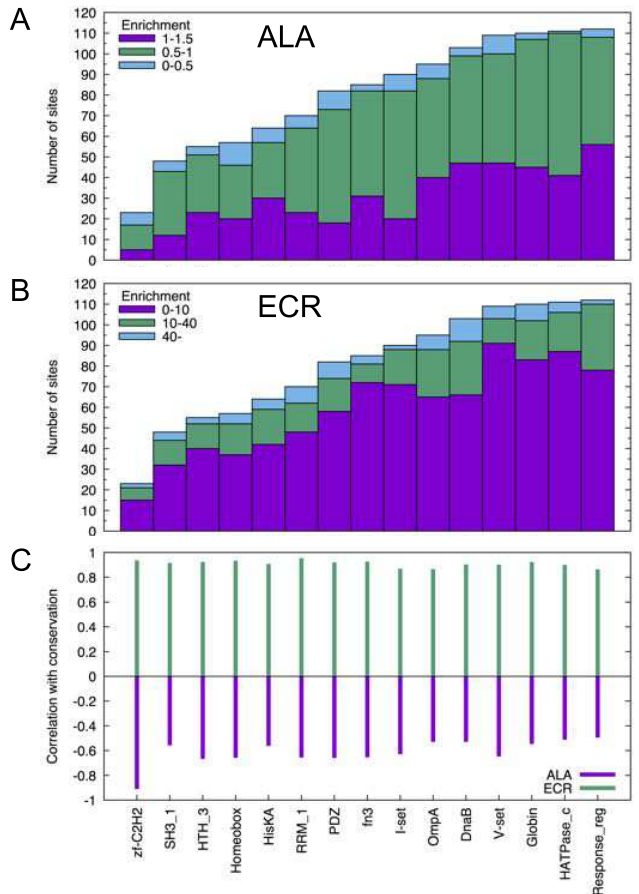


Figure 5: Virtual mutation experiments. “ALA” and “ECR” refer to “alanine mutants” (at $T = 1$) and “enforcedly conserved residues” (at $T = T_D$), respectively. The horizontal axis indicates Pfam families (see the bottom of panel C). A: Histogram of residues with specified enrichment $\text{En}_{O_i}^{ALA}$ for ALA scanning. B: Histogram of residues with specified enrichment $\text{En}_{O_i}^{ECR}$ for ECR scanning. C: Correlation between log hit ratio $\log(h_{O_i}^{ALA/ECR})$ and site conservation $D_{O_i}(T_D)$ (see Eq. 6).

3.4. Enforcing key residues promotes sequence pattern formation under disordering condition: “Enforcedly conserved residue” scanning

Conversely to alanine scanning, we can enforce the consensus (the most dominant) residue $a_{O_i}^*$ of each core site O_i by setting $\mu(O_i, a_{O_i}^*) = +20$ (and all other μ 's were set to 0) at the disordering temperature $T = T_D$. With this “enforcedly conserved residue (ECR)” mutation at each site, the hit ratio $h_{O_i}^{\text{ECR}}$ was calculated (c.f., Fig. 3C, green line) and the enrichment with respect to the standard hit ratio at T_D

$$\text{En}_{O_i}^{\text{ECR}} = h_{O_i}^{\text{ECR}} / h_0(T = T_D). \quad (10)$$

was compared (Fig. 5B). While majority of sites exhibited enrichment of less than 10 fold, a few sites showed more than 40-fold enrichment. The hit ratio for ECR mutants are even more correlated with site conservation (Fig. 5C; $R > 0.87$ for all the families). Thus, enforcing a few well-conserved residues can enhance the sequence pattern formation over the entire sequence under otherwise disordering conditions.

4. Discussion

The LGM for studying the “folding transition” in the sequence subspace around a given protein family is analogous to $G\bar{o}$ -like models for studying the folding transition in the conformational space for a given native structure ($G\bar{o}$, 1983; Clementi et al., 2000). One major conceptual difference is that while there is a unique native structure as the global energy minimum for a $G\bar{o}$ -like model, there is an *ensemble* of sequences as the global *free energy* minimum for an LGM (Eq. 4). This is because in the latter the parameters are optimized using a set of natural sequences at a finite temperature ($T = 1$). This may be considered as a consequence of the asymmetric one-to-many relationship between a protein fold and family sequences. The design of the LGM assumes a funnel-like free energy landscape of the sequence subspace analogous to that in the conformational space (Bryngelson et al., 1995). Based on simple exact models, it has been suggested that the free energy landscape of the sequence subspace within a family of sequences sharing the same ground-state conformation is indeed funnel-like (“superfunnel”) (Bornberg-Bauer and Chan, 1999; Wroe et al., 2005). The present LGM extends the superfunnel concept to include sequences slightly beyond the family boundary.

The parameters of the LGM are determined so that statistics of simulated sequences match that of an observed MSA. This may imply that the sequences sampled by the LGM may be biased towards natural sequences. Nevertheless, based on computational protein design experiments, it has been suggested that the volume of sequence space optimal for a protein structure is restricted to a region around the natural sequence (Kuhlman and Baker, 2000). Therefore, the ensemble of sequences sampled by the LGM

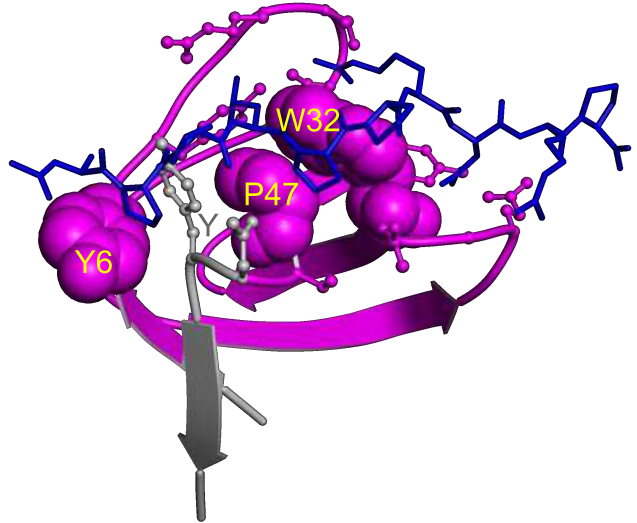


Figure 6: Chicken src SH3 domain (in magenta and grey ribbon) complexed with a proline-rich peptide (in blue sticks) (PDB: 4hvu (Bacarizo and Camara-Artigas, 2013)). The region in magenta indicates residues aligned with the Pfam profile HMM. The residues in the ball-and-stick or spacefill representations are peptide binding residues. The labeled residues in spacefill are among the key residues marked in boldface in Table 2 and they are part of the “xP pockets” (Saksela and Permi, 2012). Note there is a tyrosine residue (Y) in grey which is not aligned with the Pfam profile HMM but forms a xP pocket together with residue Y6. Figure was made with Molmil (Bekker et al., 2016).

under the natural condition is expected to be a good approximation for the ensemble of all the sequences, both natural and artificial, compatible with the protein family.

The existence of a rather sharp two-state transition implies the existence of a clear boundary between family members and non-family members. This transition is made possible by the inclusion of the long-range (non-bonded) interactions in the LGM. Conventional sequence models such as profile HMMs do not (or cannot) incorporate such long-range effects because they are essentially one-dimensional (1D) systems, and therefore, they cannot exhibit such transition (Landau and Lifshitz, 1980). Thus, the discrimination between family and non-family members based on the conventional sequence models is necessarily fuzzy, leading to false positives and false negatives. In fact, this situation may have already biased our understanding of protein families. For example, the C-terminal 3_{10} helix and β strand ($\beta 5$ in (Saksela and Permi, 2012)) of the SH3 domain are completely missing in the corresponding Pfam profile HMM (c.f., grey regions in Fig. 6), but these regions not only comprise an integral part of the SH3 fold, but also contain a functionally important tyrosine residue (Fig. 6) involved in peptide binding (Saksela and Permi, 2012).

In this study, we have used one of conventional methods, namely the profile HMM, for quantifying natural-likeness (i.e., the “hit ratio”). However, due to the limitation of profile HMMs just pointed out, such a measure may be inaccurate. In designing artificial WW domain proteins,

Table 2: Most affected sites by ALA and ECR mutations.

Pfam ID	$En_{O_i}^{ALA} < 0.5$ (ascending order) ^a	$En_{O_i}^{ECR} > 40$ (descending order) ^a
zf-C2H2	C3, H19, C6, H23 , L16, F10	C3, H19
SH3_1	Y6, W32, P47 , I1, A2	L14, F16, P47, W32
HTH_3	L1, L55, L48, L10	L15, E30, R5
Homeobox	W47, F48, R52 , L15, K56 , A53, K57 , F19, V44, L33, N50	W47, L15, F48, V44, R52
HisKA	H11 , R14, E12, L13, P16, L51, L17	P16, E12, L13, H11 , T15
RRM_1	L1, F46, L15, L6, F2, F43	F19, L15, F43 , V44, L6, A55, V3, A42
PDZ	L79, V30, L44, D48, L12 , I50, A38, L82, L16	I50, V30, L44, D48, V53, L79, A66, I70
fn3	W20, Y33, Y69	W20, V73, Y33, P3
I-set	Y71, W34, A35, L58, V90, I60, P1 , L20	W34, Y71
OmpA	R95 , F2, R53, Y1, N94, H36, L49	R53, V57, A54, F2, R95 , D38, N46
DnaB	L13, F35, L17, Y97	L13, F35, E9, F44, I43, H40, L17, V12, V62, L84, I47
V-set	Y88, V108, W33, D84, L16, L75, L109, L106, I77	Y88, W33, D84, L106, L16, L75
Globin	F38 , L24, F28	F38, F28, H59 , L24, F105, V63 , W9, G20
HATPase_c	D43	D43, N12 , V41, G76, N16
Response_reg	K100, D5 , M53, L48	D50 , M53

^aConsensus residues with core site position are listed (e.g., “C3” indicates the consensus residue C (cysteine) at core site 3, O_3 for zf-C2H2). Consensus residues involved in intermolecular interactions are marked in **boldface**. References in which intermolecular interactions were confirmed are the following: zf-C2H2 (Liu et al., 2013); SH3_1 (Bacarizo and Camara-Artigas, 2013); HTH_3 (Rodgers, 1993); Homeobox (JCSG and STEMCELL, 2014); HisKA (Marina et al., 2005); RRM_1 (Myers et al., 2003); PDZ (Tochio et al., 1999); I-set (Pernigo et al., 2010); OmpA (Xu et al., 2016); DnaB (Itsathitphaisarn et al., 2012; Lo et al., 2009); Globin (Schreiter et al., 2007); HATPase_c (Brough et al., 2009); Response_reg (Volz and Matsumura, 1991).

Socolich et al. (Socolich et al., 2005) showed that sequences designed without pairwise correlations were unable to fold whereas all the designed foldable proteins were designed with pairwise correlations (by statistical coupling analysis (Lockless and Ranganathan, 1999)). It has been shown that other statistical models incorporating “direct” long-range correlations can discriminate foldable sequences from unfoldable ones to a very good accuracy (Balakrishnan et al., 2011; Cocco et al., 2017) for the artificially designed WW domains (Socolich et al., 2005). The LGM also incorporates the direct long-range correlations in the form of interacting non-bonded pairs so its energy value is expected to be a good discriminator of foldable proteins. It is of interest and in principle possible to experimentally measure the foldability of the sequences generated by the LGM.

In the context of molecular evolution, the present results imply that if some selective pressure is imposed on one or a few key sites, the entire sequence may evolve rather quickly to form a pattern compatible with the family which is characterized by a unique fold. How can such selective pressure act on residues that are to be conserved? According to recent studies, there is strong evidence that protein families have been naturally (and positively) selected so as to stabilize their native folds (Morcos et al., 2014; Miyazawa, 2017). In fact, most of the key residues listed in Table 5 comprise the structural core of native folds. Furthermore, visual inspection of native structures in Table 1 and their homologs revealed that the key residues often in-

cluded those involved in intermolecular interactions such as small molecule, polypeptide/protein or polynucleotide binding, or phosphorylation (Table 2). For example, in the case of the SH3 domain (Fig. 6), the key residues Y6, W32 and P47 (consensus residues according to Fig. 3A) comprise the “xP pockets” essential for the proline-rich peptide binding activity (Bacarizo and Camara-Artigas, 2013; Saksela and Permi, 2012). Thus, some functionally important residues play an essential role in shaping the pattern of family sequences and hence the native fold (Yomo et al., 1999) although they may not be necessarily optimal with respect to structural stability (Ota et al., 2003). This may also help explain the observation that most of the structural motifs for ligand binding sites are confined within single protein families (Kinjo and Nakamura, 2009, 2010).

5. Materials and Methods

5.1. Data preparation

Multiple sequence alignments (MSA) and profile hidden Markov models (HMMs) were downloaded from the Pfam database (version 30.0). The MSAs were based on the “uniprot” set when available or on the largest available representative set, otherwise (Table 1). Aligned sequences that contained more than or equal to 10% deleted residues on core sites were discarded. A representative structure of each family was assigned based on resolution and alignment quality using the PDBj Mine2 relational database (Kinjo et al., 2012, 2017a,b) integrated with the SIFTS (Velankar et al., 2013) resource (Table 1).

5.2. Monte Carlo simulations

In each MC simulation of a LGM model of length N , one sweep consists of N and $N - 1$ attempted mutations for randomly selected core and insert sites, respectively. For the results given in Figs. 2B, C and 5, 20 grand canonical MC simulations (Kinjo, 2017) (under the conditions described in the text) were performed for 10^6 sweeps after 5×10^4 sweeps of equilibration, and 10,000 sequences (alignments) were saved every 100 steps for each of the 20 trajectories. For each set of 10,000 sequences resulted from each trajectory, a sequence database was created by removing the “delete” symbols from the sequences, against which the *hmmsearch* (Eddy, 2011) program was applied with the Pfam profile HMM with the E-value cutoff of 0.01 in order to identify significantly similar sequences. From the 20 runs, the average hit ratio and the standard deviation were obtained.

For the results given in Figs. 2A, 3, and 4, first, the density of states was determined by the Wang-Landau method (Wang and Landau, 2001) by using the energy bins with bin width of 0.2 energy units. The lower bound of the energy range was fixed at a sufficiently low value, and the upper bound was determined by tentative grand canonical MC simulations at a high temperature $T = 1.2$. The Wang-Landau iteration was terminated when the density of states was determined to the precision better than 10^{-7} . Next, using thus determined density of states, a multicanonical MC simulation (Berg and Neuhaus, 1992) was performed until all the energy bins are filled with at least 2,000 counts (sequences were saved at every sweep). From this trajectory, the specific heat and residue distributions at various temperatures were obtained by the reweighting method (Newman and Barkema, 1999).

6. Acknowledgements

The author thanks Ken Nishikawa, Motonori Ota and Gautam Basu for valuable comments.

References

Bacarizo, J., Camara-Artigas, A., 2013. Atomic resolution structures of the c-Src SH3 domain in complex with two high-affinity peptides from classes I and II. *Acta Crystallogr. D* 69, 756–766.

Balakrishnan, S., Kamisetty, H., Carbonell, J. G., Lee, S. I., Langmead, C. J., 2011. Learning generative models for protein fold families. *Proteins* 79, 1061–1078, doi:10.1002/prot.22934.

Bastolla, U., Roman, H. E., Vendruscolo, M., 1999. Neutral evolution of model proteins: diffusion in sequence space and overdispersion. *J. Theor. Biol.* 200, 49–64.

Bekker, G.-J., Nakamura, H., Kinjo, A. R., 2016. Molmil: a molecular viewer for the PDB and beyond. *J. Cheminform.* 8, 42, doi: 10.1186/s13321-016-0155-1.

Berg, B., Neuhaus, T., 1992. Multicanonical ensemble: A new approach to simulate first-order phase transitions. *Phys. Rev. Lett.* 68, 912.

Berman, H., Henrick, K., Nakamura, H., Markley, J. L., 2007. The worldwide Protein Data Bank (wwPDB): ensuring a single, uniform archive of PDB data. *Nucleic Acids Res.* 35, D301–D303.

Biswas, T., Tsodikov, O. V., 2008. Hexameric ring structure of the N-terminal domain of *Mycobacterium tuberculosis* DnaB helicase. *FEBS J.* 275, 3064–3071.

Bornberg-Bauer, E., 1997. How are model protein structures distributed in sequence space? *Biophys. J.* 73, 2393–2403.

Bornberg-Bauer, E., Chan, H. S., 1999. Modeling evolutionary landscapes: Mutational stability, topology, and superfunnels in sequence space. *Proc. Natl. Acad. Sci. USA* 96, 10689–10694.

Brough, P. A., Barril, X., Borgognoni, J., Chene, P., Davies, N. G. M., Davis, B., Drysdale, M. J., Dymock, B., Eccles, S. A., Garcia-Echeverria, C., Fromont, C., Hayes, A., Hubbard, R. E., Jordan, A. M., Jensen, M. R., Massey, A., Merrett, A., Padfield, A., Parsons, R., Radimerski, T., Raynaud, F. I., Robertson, A., Roughley, S. D., Schoepfer, J., Simmonite, H., Sharp, S. Y., Surgenor, A., Valenti, M., Walls, S., Webb, P., Wood, M., Workman, P., Wright, L. M., 2009. Combining hit identification strategies: Fragment-based and in silico approaches to orally active 2-aminothieno[2,3-D]pyrimidine inhibitors of the Hsp90 molecular chaperone. *J. Med. Chem.* 52, 4794–4809.

Brumshtein, B., Esswein, S. R., Landau, M., Ryan, C. M., Whitelegge, J. P., Phillips, M. L., Cascio, D., Sawaya, M. R., Eisenberg, D. S., 2014. Formation of amyloid fibers by monomeric light-chain variable domains. *J. Biol. Chem.* 289, 27513–27525.

Bryngelson, J. D., Onuchic, J. N., Socci, N. D., Wolynes, P. G., 1995. Funnels, pathways, and the energy landscape of protein folding: A synthesis. *Proteins: Structure, Function, and Bioinformatics* 21, 167–195.
URL <http://dx.doi.org/10.1002/prot.340210302>

Cheng, H., Schaeffer, R. D., Liao, Y., Kinch, L. N., Pei, J., Shi, S., Kim, B.-H., Grishin, N. V., 12 2014. Ecod: An evolutionary classification of protein domains. *PLOS Computational Biology* 10, 1–8.
URL <https://doi.org/10.1371/journal.pcbi.1003926>

Clementi, C., Nymeyer, H., Onuchic, J., 2000. Topological and energetic factors: what determines the structural details of the transition state ensemble and “en-route” intermediates for protein folding? an investigation for small globular proteins. *J. Mol. Biol.* 298, 937–953.

Cocco, S., Feinauer, C., Figliuzzi, M., Monasson, R., Weigt, M., 2017. Inverse Statistical Physics of Protein Sequences: A Key Issues Review. *ArXiv e-prints*, q-bio.BM/1703.01222.

Eddy, S. R., 2011. Accelerated profile HMM searches. *PLoS Comput. Biol.* 7, e1002195.

Finn, R. D., Bateman, A., Clements, J., Coggill, P., Eberhardt, R. Y., Eddy, S. R., Heger, A., Hetherington, K., Holm, L., Mistry, J., Sonnhammer, E. L. L., Tate, J., Punta, M., 2014. The Pfam protein families database. *Nucleic Acids Res.* 42, D222–D230, doi:10.1093/nar/gkt1223.

Gō, N., 1983. Theoretical studies of protein folding. *Annu. Rev. Biophys. Bioeng.* 12, 183–210.

Goldstein, R. A., 2008. The structure of protein evolution and the evolution of protein structure. *Curr. Opin. Struct. Biol.* 18, 170–177.

Govindarajan, S., Goldstein, R. A., 1995. Searching for foldable protein structures using optimized energy functions. *Biopolymers* 36, 43–51.

Govindarajan, S., Goldstein, R. A., 1996. Why are some protein-structures so common? *Proc. Natl. Acad. Sci. USA* 93, 3341–3345.

Gribskov, M., McLachlan, A. D., Eisenberg, D., 1987. Profile analysis: detection of distantly related proteins. *Proc. Natl. Acad. Sci. U.S.A.* 84, 4355–4358.

Holzgräfe, C., Wallin, S., 2014. Smooth functional transition along a mutational pathway with an abrupt protein fold switch. *Biophys. J.* 107, 1217–1225.

Itsathitphaisarn, O., Wing, R. A., Eliason, W. K., Wang, J., Steitz, T. A., 2012. The hexameric helicase DnaB adopts a nonplanar conformation during translocation. *Cell* 151, 267–277.

JCSG, STEMCELL, 2014. Crystal structure of a distal-less homeobox protein 5 (Dlx5) from *Homo sapiens* at 1.85 Å resolution. PDB: 4RDU.

Jones, D. T., Buchan, D. W., Cozzetto, D., Pontil, M., 2012. PSI-

- COV: precise structural contact prediction using sparse inverse covariance estimation on large multiple sequence alignments. *Bioinformatics* 28, 184–190, doi:10.1093/bioinformatics/btr638.
- Karthikeyan, S., Leung, T., Birrane, G., Webster, G., Ladias, J. A., 2001. Crystal structure of the PDZ1 domain of human Na(+)/H(+) exchanger regulatory factor provides insights into the mechanism of carboxyl-terminal leucine recognition by class I PDZ domains. *J. Mol. Biol.* 308, 963–973.
- Kinjo, A. R., 2015. Liquid-theory analogy of direct-coupling analysis of multiple-sequence alignment and its implications for protein structure prediction. *Biophys. Physicobiol.* 12, 117–119.
- Kinjo, A. R., 2016. A unified statistical model of protein multiple sequence alignment integrating direct coupling and insertions. *Biophys. Physicobiol.* 13, 45–62.
- Kinjo, A. R., 2017. Monte Carlo simulation of a statistical mechanical model of multiple protein sequence alignment. *Biophys. Physicobiol.* 14, 99–110.
- Kinjo, A. R., Bekker, G.-J., Suzuki, H., Tsuchiya, Y., Kawabata, T., Ikegawa, Y., Nakamura, H., 2017a. Protein Data Bank Japan (PDBj): Updated user interfaces, resource description framework, analysis tools for large structures. *Nucleic Acids Res.* 45, D282–D288.
- Kinjo, A. R., Bekker, G.-J., Wako, H., Endo, S., Tsuchiya, Y., Sato, H., Nishi, H., Kinoshita, K., Suzuki, H., Kawabata, T., Yokochi, M., Iwata, T., Kobayashi, N., Fujiwara, T., Kurisu, G., Nakamura, H., 2017b. New tools and functions in data-out activities at Protein Data Bank Japan (PDBj). *Protein Sci.* in press, doi:10.1002/pro.3273.
- Kinjo, A. R., Horimoto, K., Nishikawa, K., 2005. Predicting absolute contact numbers of native protein structure from amino acid sequence. *Proteins* 58, 158–165, doi:10.1002/prot.20300.
- Kinjo, A. R., Nakamura, H., 2008. Nature of protein family signatures: insights from singular value analysis of position-specific scoring matrices. *PLoS One* 3, e1963, doi:10.1371/journal.pone.0001963.
- Kinjo, A. R., Nakamura, H., 2009. Comprehensive structural classification of ligand binding motifs in proteins. *Structure* 17, 234–246.
- Kinjo, A. R., Nakamura, H., 2010. Geometric similarities of protein-protein interfaces at atomic resolution are only observed within homologous families: an exhaustive structural classification study. *J. Mol. Biol.* 399, 526–540.
- Kinjo, A. R., Suzuki, H., Yamashita, R., Ikegawa, Y., Kudo, T., Igarashi, R., Kengaku, Y., Cho, H., Standley, D. M., Nakagawa, A., Nakamura, H., 2012. Protein Data Bank Japan (PDBj): Maintaining a structural data archive and resource description framework format. *Nucleic Acids Res.* 40, D453–D460.
- Koehl, P., Levitt, M., 2002. Protein topology and stability define the space of allowed sequences. *Proc. Natl. Acad. Sci. USA* 99, 1280–1285.
- Kuhlman, B., Baker, D., 2000. Native protein sequences are close to optimal for their structures. *Proc. Natl. Acad. Sci. USA* 97, 10383–10388.
- Landau, L. D., Lifshitz, E. M., 1980. *Statistical Physics, Part I*, 3rd Edition. Iwanami Shoten, Tokyo, Japanese translation.
- Lapedes, A. S., Giraud, B., Liu, L., Stormo, G. D., 1999. Correlated mutations in models of protein sequences: phylogenetic and structural effects. *Statistics in molecular biology and genetics (IMS Lecture Notes–Monograph Series)* 33, 236–256.
- Levy, R. M., Haldane, A., Flynn, W. F., 2017. Potts hamiltonian models of protein co-variation, free energy landscapes, and evolutionary fitness. *Curr. Opin. Struct. Biol.* 43, 55 – 62.
- Li, H., Helling, R., Tang, C., Wingreen, N., 1996. Emergence of preferred structures in a simple model of protein folding. *Science* 273, 666–669.
- Li, S., Li, T., Xu, Y., Zhang, Q., Zhang, W., Che, S., Liu, R., Wang, Y., Bartlam, M., 2015. Structural insights into YfiR sequestering by YfiB in *Pseudomonas aeruginosa* PAO1. *Sci. Rep.* 5, 16915.
- Liu, Y., Olanrewaju, Y. O., Zhang, X., Cheng, X., 2013. DNA recognition of 5-carboxylcytosine by a zfp57 mutant at an atomic resolution of 0.97 angstrom. *Biochemistry* 52, 9310–9317.
- Lo, Y. H., Tsai, K. L., Sun, Y. J., Chen, W. T., Huang, C. Y., Hsiao, C. D., 2009. The crystal structure of a replicative hexameric helicase *dnac* and its complex with single-stranded DNA. *Nucleic Acids Res.* 37, 804–814.
- Lockless, S. W., Ranganathan, R., 1999. Evolutionarily conserved pathways of energetic connectivity in protein families. *Science* 286, 295–299, doi: 10.1126/science.286.5438.295.
- MacKay, D. J. C., 2003. *Information Theory, Inference, and Learning Algorithms*. Cambridge University Press, Cambridge, UK.
- Manjasetty, B. A., Niesen, F. H., Scheich, C., Roske, Y., Gotz, F., Behlke, J., Sievert, V., Heinemann, U., Bussow, K., 2005. X-ray structure of engineered human aortic preferentially expressed protein-1 (APEG-1). *BMC Struct. Biol.* 5, 21.
- Marina, A., Waldburger, C. D., Hendrickson, W. A., 2005. Structure of the entire cytoplasmic portion of a sensor histidine-kinase protein. *Embo J.* 24, 4247–4259.
- Maynard Smith, J., 1970. Natural selection and the concept of a protein space. *Nature* 225, 563–564.
- McLellan, J. S., Yao, S., Zheng, X., Geisbrecht, B. V., Ghirlando, R., Beachy, P. A., Leahy, D. J., 2006. Structure of a heparin-dependent complex of Hedgehog and Ihog. *Proc. Natl. Acad. Sci. USA* 103, 17208–17213.
- Miyazawa, S., 2013. Prediction of contact residue pairs based on co-substitution between sites in protein structures. *PLoS One* 8, e54252, doi:10.1371/journal.pone.0054252.
- Miyazawa, S., 2017. Selection originating from protein stability/foldability: Relationships between protein folding free energy, sequence ensemble, and fitness. *J. Theor. Biol.* in press.
- Mondragon, A., Subbiah, S., Almo, S. C., Drottler, M., Harrison, S. C., 1989. Structure of the amino-terminal domain of phage 434 repressor at 2.0 Å resolution. *J. Mol. Biol.* 205, 189–200.
- Morcos, F., Pagnani, A., Lunt, B., Bertolino, A., Marks, D. S., Sander, C., Zecchina, R., Onuchic, J. N., Hwa, T., Weigt, M., 2011. Direct-coupling analysis of residue coevolution captures native contacts across many protein families. *Proc. Natl. Acad. Sci. USA* 108, E1293–E1301.
- Morcos, F., Schafer, N. P., Cheng, R. R., Onuchic, J. N., Wolynes, P. G., 2014. Coevolutionary information, protein folding landscapes, and the thermodynamics of natural selection. *Proc. Natl. Acad. Sci. USA* 111, 12408–12413.
- Murzin, A. G., Brenner, S. E., Hubbard, T., Chothia, C., 1995. SCOP: A structural classification of proteins database for the investigation of sequences and structures. *J. Mol. Biol.* 247, 536–540.
- Myers, J. C., Moore, S. A., Shamoo, Y., 2003. Structure-based incorporation of 6-methyl-8-(2-deoxy-beta-ribofuranosyl)isoxanthopterin into the human telomeric repeat DNA as a probe for UP1 binding and destabilization of G-tetrad structures. *J. Biol. Chem.* 278, 42300–42306.
- Newman, M. E. J., Barkema, G. T., 1999. *Monte Carlo Methods in Statistical Physics*. Clarendon Press, Oxford, UK.
- Nishikawa, K., 1993. Island hypothesis: protein distribution in the sequence space. *Viva Origino* 21, 91–102.
- Nishikawa, K., 2002. Information concept in biology. *Bioinformatics* 18, 649–651.
- Orengo, C. A., Michie, A. D., Jones, S., Jones, D. T., Swindells, M. B., Thornton, J. M., 1997. CATH - a hierarchic classification of protein domain structures. *Structure* 5, 1093–1108.
- Ota, M., Kinoshita, K., Nishikawa, K., 2003. Prediction of catalytic residues in enzymes based on known tertiary structure, stability profile, and sequence conservation. *J. Mol. Biol.* 327, 1053–1064.
- Pande, V. S., Grosberg, A. Y., Tanaka, T., 2000. Heteropolymer freezing and design: Towards physical models of protein folding. *Rev. Mod. Phys.* 72, 259314.
- Pernigo, S., Fukuzawa, A., Bertz, M., Holt, M., Rief, M., Steiner, R., Gautel, M., 2010. Structural insight into M-band assembly and mechanics from the titin-obscure-like-1 complex. *Proc. Natl. Acad. Sci. USA* 107, 2908–2913.
- Raman, S., Singh, M., Tatu, U., Suguna, K., 2015. First structural view of a peptide interacting with the nucleotide binding domain of heat shock protein 90. *Sci. Rep.* 5, 17015.
- Rodgers, D. W. and Harrison, S. C., 1993. The complex between phage 434 repressor DNA-binding domain and operator site OR3:

- structural differences between consensus and non-consensus half-sites. *Structure* 1, 227–240.
- Saksela, K., Permi, P., 2012. SH3 domain ligand binding: What's the consensus and where's the specificity? *FEBS Lett.* 586, 2609–2614, doi: 10.1016/j.febslet.2012.04.042.
- Schreiter, E., Rodriguez, M., Weichsel, A., Montfort, W., Bonaventura, J., 2007. S-nitrosylation-induced conformational change in blackfin tuna myoglobin. *J. Biol. Chem.* 282, 19773–19780.
- Shakhnovich, E. I., Gutin, A. M., 1993. Engineering of stable and fast-folding sequences of model proteins. *Proc. Natl. Acad. Sci. USA* 90, 7195–7199.
- Sikosek, T., Krobath, H., Chan, H. S., 2016. Theoretical insights into the biophysics of protein bi-stability and evolutionary switches. *PLoS Comput. Biol.* 12, e1004960.
- Socolich, M., Lockless, S. W., Lee, H. L., Gardner, K., Ranganathan, R., 2005. Evolutionary information for specifying a protein fold. *Nature* 437, 512–518.
- Sutto, L., Marsili, S., Valencia, A., Gervasio, F. L., 2015. From residue coevolution to protein conformational ensembles and functional dynamics. *Proc. Natl. Acad. Sci. USA* 112 (44), 13567–13572.
- Taylor, W. R., 1986. Identification of protein sequence homology by consensus template alignment. *J. Mol. Biol.* 188, 233–258.
- Taylor, W. R., Jones, D. T., Sadowski, M. I., 2012. Protein topology from predicted residue contacts. *Prot. Sci.* 21, 299–305.
- Tochio, H., Zhang, Q., Mandal, P., Li, M., Zhang, M., 1999. Solution structure of the extended neuronal nitric oxide synthase PDZ domain complexed with an associated peptide. *Nat. Struct. Biol.* 6, 417–421.
- Velankar, S., Dana, J. M., Jacobsen, J., van Ginkel, G., Gane, P. J., Luo, J., Oldfield, T. J., O'Donovan, C., Martin, M. J., Kleywegt, G. J., 2013. SIFTS: Structure integration with function, taxonomy and sequences resource. *Nucleic Acids Res.* 41, D483–D489, doi: 10.1093/nar/gks1258.
- Vitali, J., Ding, J., Jiang, J., Zhang, Y., Krainer, A. R., Xu, R. M., 2002. Correlated alternative side chain conformations in the RNA-recognition motif of heterogeneous nuclear ribonucleoprotein A1. *Nucleic Acids Res.* 30, 1531–1538.
- Volz, K., Matsumura, P., 1991. Crystal structure of *Escherichia coli* CheY refined at 1.7-Å resolution. *J. Biol. Chem.* 266, 15511–15519.
- Wang, F., Landau, D. P., 2001. Efficient, multiple-range random walk algorithm to calculate the density of states. *Phys. Rev. Lett.* 86, 2050–2053.
- Wroe, R., Bornberg-Bauer, E., Chan, H. S., 2005. Comparing folding codes in simple heteropolymer models of protein evolutionary landscape: Robustness of the superfunnel paradigm. *Biophys. J.* 88, 118–131.
- Wroe, R., Chan, H. S., Bornberg-Bauer, E., 2007. A structural model of latent evolutionary potentials underlying neutral networks in proteins. *HFSP J.* 1, 79–87.
- Xu, M., Yang, X., Yang, X.-A., Zhou, L., Liu, T.-Z., Fan, Z., Jiang, T., 2016. Structural insights into the regulatory mechanism of the *Pseudomonas aeruginosa* YfiBNR system. *Protein Cell* 7, 403–416.
- Yomo, T., Saito, S., Sasai, M., 1999. Gradual development of protein-like global structures through functional selection. *Nat. Struct. Biol.* 6, 743–746.